Journal of Biomaterials Applications

http://jba.sagepub.com

In Vitro Study on Different Cell Response to Spherical Hydroxyapatite Nanoparticles

Qiang Fu, Mohamed N. Rahaman, Nai Zhou, Wenhai Huang, Deping Wang, Liying Zhang and Haifeng Li

J Biomater Appl 2008; 23; 37 originally published online Jan 14, 2008;
DOI: 10.1177/0885328207081350

The online version of this article can be found at:
http://jba.sagepub.com/cgi/content/abstract/23/1/37

Published by:
SAGE
http://www.sagepublications.com

In Vitro Study on Different Cell Response to Spherical Hydroxyapatite Nanoparticles

QIANG FU,[1,2,*] MOHAMED N. RAHAMAN,[1] NAI ZHOU,[2] WENHAI HUANG,[2,3,*] DEPING WANG,[2] LIYING ZHANG[2] AND HAIFENG LI[4]

[1]*Department of Materials Science and Engineering University Missouri-Rolla, 223 McNutt Hall, Rolla, Missouri 65409, USA*

[2]*School of Materials Science and Engineering, Tongji University Shanghai 200092, China*

[3]*Materials Research Center, University of Missouri-Rolla 101 Straumanis Hall, Rolla, MO 65409, USA*

[4]*Tongji Hospital Affiliated Tongji University, Shanghai, 200065, China*

ABSTRACT: Hydroxyapatite (HA) is widely used in filling of bone defects and coating on metal parts of prosthetic implants due to its excellent biocompatibility, bioactivity, and bone-bonding properties. It has been demonstrated that micro-sized HA particles cause inflammatory reaction, especially for the needle shaped particles. However, little effort has been concentrated on the cell responses of the spherical HA nanoparticles. The aim of the present work is to chemically and physically characterize the synthesized HA nanoparticles and to investigate the *in vitro* cell responses. X-ray diffraction, electron microscopy, nitrogen adsorption, and Fourier transform infrared spectroscopy revealed that the particles consisted of nearly spherical crystallites of carbonate-substituted HA with size of 20–40 nm and specific surface area of 75 m^2/g. L929 cell proliferation experiments demonstrate that the spherical HA nanoparticles is more biocompatible than commercially available HA. On the other hand, U2-OS cell test results show that the inhibition rate of the spherical HA nanoparticles increases with time and concentration. The half effective inhibitory concentration (IC50) of the nanoparticles was determined to be 50.8 μg/mL at 72 h. All these data indicated that the synthesized spherical nanocrystalline

*Authors to whom correspondence should be addressed. E-mails: qf7r9@umr.edu; whhuang@mail.tongji.edu.cn

0885-3282/08/01 0037–14 $10.00/0 DOI: 10.1177/0885328207081350

Los Angeles, London, New Delhi and Singapore

HA particles can function as an effective biomaterial for bone tumorectomy repair, while having little adverse effect.

KEY WORDS: nanocrystalline hydroxyapatite, cell proliferation, cell responses, biomaterials, L929 cell line.

INTRODUCTION

As a desirable bone replacement material, hydroxyapatite (HA), with the stoichiometric composition $Ca_{10}(PO_4)_6(OH)_2$), has received significant attention for use in the repair of bone defects and coating on metal parts of prosthetic implants due to its excellent biocompatibility, bioactivity, and bone-bonding properties [1–4]. Extensive studies have been carried out using cell culture techniques [5–7] and *in vivo* [8–12]. Due to the similarity of the size of nano-sized HA with the HA crystal in natural bone, a lot of work has been done on the synthesis of HA nanoparticles [13–18]. Cautions should be exercised before using these nanoparticles, as the size, morphology, and structure of HA particles have significant effect on the biological response [19–25]. Hydroxyapatite nanoparticles may significantly decrease the transforming growth factor-β1 (TGF-β1) concentration and increase the prostaglandin E_2 (PGE_2) concentration [19,20].

Recent research has shown that nanocrystalline HA particles inhibited the growth and proliferation of several types of cancer cells, including liver and throat cells, while having little side effects on normal cells. Li [26] found that ultrafine HA particles, added to the cell culture medium, inhibited the growth of MGC-803 cells. He observed disorganization of microtubules and disruption of stress fiber in the cells treated with HA. It was believed that the ultrafine HA particles changed the morphology of the MGC-803 cells, which eventually affected the cytoskeleton of the cells. The effect of HA nanoparticles on the human hepatoma cell line BEL-7402 was investigated by Liu et al. [27], who found that particles inhibited cell growth in a dose-dependent manner, with the half effective inhibitory concentration (IC50) of 29.3 mg/L. Our recent work also has shown a type of spherical nano HA particle that has an effective inhibition on U2-OS cancer cells. An inhibition rate of 73.4 ± 3.1 was determined for the nano HA suspension of 250 μg/mL [28,29]. However, despite the studies on the inhibitory effect on cancer cells, no work on the cytocompatibility evaluation of spherical HA nanoparticles has

been reported. Due to the possible toxicity, it is of great importance to investigate the chemical composition and physical properties of HA nanoparticles and hence *in vitro* cell responses.

In the present work, the synthetic HA nanoparticles were chemically and physically characterized to obtain an understanding of the particles from a Materials Science point of view. To evaluate the cytocompatibility of the synthesized particle, MTT (3-{4,5-dimethylthiazol-2yl}-2,5-diphenyltetrazolium bromide) method was performed using a cell line of L929. In addition, the concentration effect of nano HA suspension on U2-OS cell line was determined.

MATERIALS AND METHODS

Synthesis and Characterization of Spherical Nanocrystalline HA Particles

Commercially available HA was obtained from Shanghai Chemical Corporation, China. The spherical nanocrystalline HA particles was synthesized from $Ca(NO_3)_2\ 2H_2O$ and $(NH_4)_2HPO_4$ using the method described in our previous work [28].

Crystalline phases in the synthesized powder were detected by X-ray diffraction, XRD (D/mas 2550v, Rigaku, Tokyo, Japan) using Cu K_α radiation ($\lambda = 0.15406$ nm) in a step-scan mode (0.02° per step) in the range of 10–80° 2θ. The surface area of the as-dried HA powder was determined by the Brunauer, Emmet and Teller, BET method (NOVA 1000, Quantachrome, Boynton Beach, FL). Scanning electron microscopy, SEM (Hitachi S-4700) was used to observe the size and morphology of the as-dried HA. Fourier transform infrared (FTIR) analysis (FTX-40 Biorad; Digilab, Cambridge, MA) of the dried nanocrystalline HA powder was performed in the wavenumber range of 400–4000 cm^{-1}. A few micrograms of the powder was mixed with KBr and pressed into pellets for the FTIR analysis.

Cell Cultures

Mouse fibroblasts (L929) from the Institute of Cell Biology, Chinese Academy of Science, Shanghai, China were cultured in Dulbecco's modified Eagle's medium (DMEM) supplemented with 10% fetal bovine serum (FBS, Gibco, USA), 2 mM glutamine, 1 mM sodium pyruvate, 100 μg/mL of penicillin, 100 μg/mL of streptomycin, and 50 μg/mL of

ascorbic acid. Once 80% confluence was reached, the cells were subcultured for cytotoxicity study.

Osteosarcoma U2-OS cells, obtained from the Institute of Cell Biology, Chinese Academy of Science, Shanghai, China, were cultured (3000 cells/mL) in Roswell Park Memorial Institute (RPMI) medium 1640 (Gibco, NY, USA) supplemented with 10% fetal bovine serum (FBS, Gibco, USA), 2 mM glutamine, 1 mM sodium pyruvate, 100 μg/mL of penicillin, 100 μg/mL of streptomycin, and 50 μg/mL of ascorbic acid.

MTT Assay

The MTT colorimetric assay is a preliminary screening test for the indirect estimation of mitochondrial oxidative processes of living cells. It measures the reduction of the tetrazolium salt into insoluble colored formazan crystals [30,31].

In the present work, both U2-OS cells and L929 cells were seeded in a 96-well culture plate, 0.2 mL in each well, and maintained at 37°C in a fully humidified atmosphere at 5% CO_2 in air for 24 h. The medium in the control groups was then replaced by fresh medium, whereas the medium in the trial groups was replaced by RPMI medium 1640 containing different concentrations of nanocrystalline and commercial HA particles. The suspensions of HA particles were prepared by first mixing the particles in the RPMI medium to give a stock suspension with a concentration of 250 μg/mL, then diluting the stock suspension, as necessary, to give suspensions with particle concentrations of 31.25–250 μg/mL.

Cell proliferation was measured using the MTT test (3-(4, 5-dimethyl-2-thya-zolyl)-2, 5-diphenyl-2H-tetrazolium-bromide; Merck, Schuchardt, Germany) after 1, 2, and 3 days. The medium was removed and 0.2 mL MTT solution was added to each well. After incubation for 4 h at 37°C in a fully humidified atmosphere of 5% CO_2 in air, the untransformed MTT was removed and 0.3 mL of isopropanol was added. The optical density (OD) was measured using ELISA (enzyme-linked immunosorbent assays) reader (EL311SX AutoReader; Bio-Tek Instruments, Winooski, VT, USA) at a wavelength of 570 nm. A mean value was obtained from measurements on eight samples. The inhibition resulting from the nanocrystalline HA was determined from the formula:

$$\text{Inhibition factor} = \frac{\text{OD of control group} - \text{OD of trial group}}{\text{OD of control group}} \times 100\% \quad (1)$$

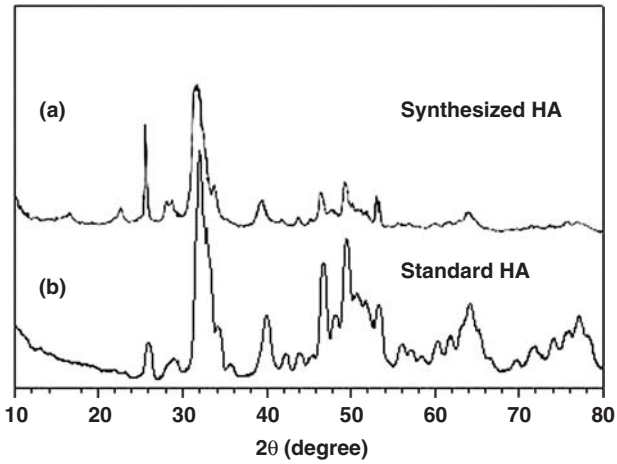

Figure 1. XRD pattern of HA powder prepared by chemical precipitation from solution (a). For comparison, the pattern of a standard HA (JCPDS 72-1243) is also shown (b).

Three samples from each trial group or control were processed for observation in the TEM. Cells grown on the material were fixed for 1 h in 2.5% glutaraldehyde containing pH 7.4 phosphate buffer (0.01 M), then dehydrated at a graded ethanol series. The samples were washed four times in liquid CO_2 and subjected to critical point dehydration in a CO_2 atmosphere (80 atm at 33°C). The cell morphology and structure were observed using TEM (Hitachi H600).

Statistical Analysis

Values, expressed as the mean ± standard deviation (SD), were compared using two-way ANOVA. Subsequently, possible differences were investigated in a *post hoc* test using Fisher's protected least significant difference (Fisher's PLSD, Stat View, Version 4.02, Apple Corporation). Differences at $p < 0.05$ were considered to be statistically significant.

RESULTS AND DISCUSSION

Characteristics of Synthesized Hydroxyapatite particles

The XRD pattern (Figure 1) indicates that the synthesized particles have a crystal structure corresponding to that of a standard HA

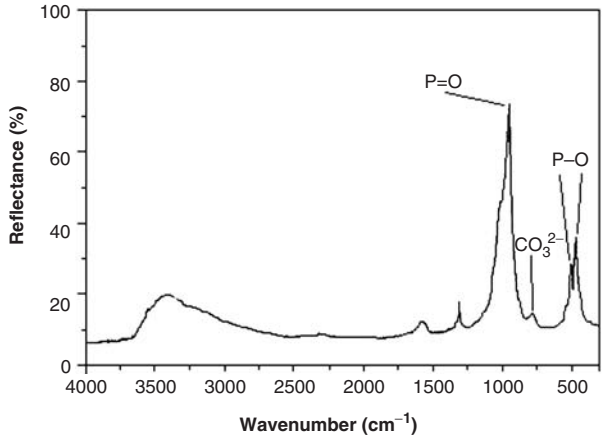

Figure 2. FTIR spectrum of the synthesized HA powder.

(Bio-Rad Laboratories, CA 94547, USA, JCPDS 72-1243). However, the smaller intensity (height) of the main diffraction peak at ~33° 2θ, when compared to the standard, is an indication that the synthesized HA particles might be only weakly crystalline. The FTIR spectrum (Figure 2) of the synthesized powder reveals peaks at wavenumbers of 1420 cm^{-1} and 1450 cm^{-1} corresponding to the splitting of CO_3^{2-} groups incorporated into the HA crystal [32]. Peaks present at wavenumbers of 560 cm^{-1} and 602 cm^{-1} correspond to the bending vibration of the P–O bond, whereas the peak at 1080 cm^{-1} corresponds to the stretching vibration of the P=O bond. The FTIR data indicate that the synthesized HA particles have carbonate groups substituted into the structure [33]. The substitution of carbonate groups for phosphate groups occurs readily in HA [34,35]. In the present experiments, the carbonate substitution may result from CO_2 in the atmosphere, dissolved in the solutions used for the preparation of the HA particles [36].

BET results show that as-dried HA has a high specific surface area, 75 m^2/g, which implies that the synthesized HA may have a high activity. The SEM micrograph in Figure 3(a) shows a slightly agglomerated mass of fine and nearly equiaxial particles with the size of 20–40 nm. A high resolution SEM image shows that the particles are nearly spherical (Figure 3(b)). In combination, XRD, FTIR, and electron microscopy indicate that the synthesized particles consist of weakly crystalline, nano-sized particles of carbonate-substituted HA.

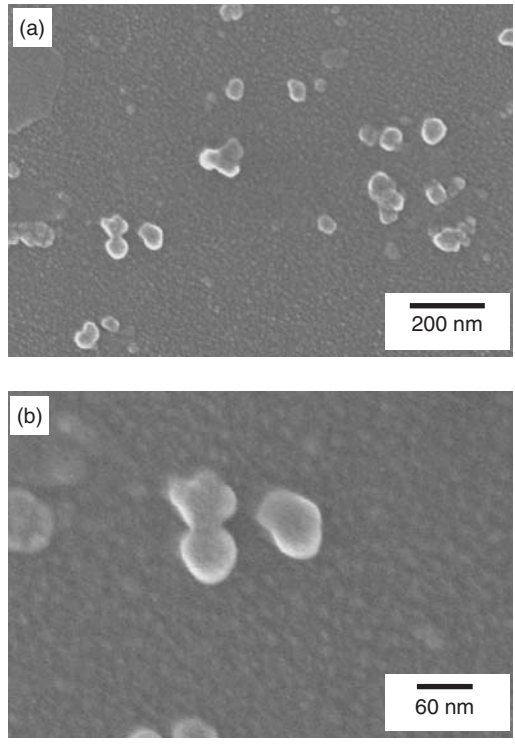

Figure 3. Micrographs of the synthesized power observed by SEM (a) ×90,000; and (b) ×200,000.

Cytotoxicity of Spherical HA Nanoparticles

It has been reported that the physical characteristics (size, shape, and sintering temperature) of the HA particles could modify the toxicity of the material and the cytokines produced by various cells [19–25]. The HA particles shape has been demonstrated to have significant influence on the cell response. Among the three studies of shapes (spherical, irregular, and needle), the needle particles always induced the most important expression and production of inflammatory cytokines and hence the most inflammatory reaction [23,25]. Also, irregularly shaped particles produced a greater response than spherical particles. The toxicity of the needle shape particles were thought to be due to the particle–cell interaction caused by mechanical stresses on the cell surface [37,38].

Although some recent work has been done on the different cell response and toxicity of small-sized HA particles, these studies focused on micron-sized particles and few researches have been conducted on the nano-sized particles, which is the main inorganic component of human bones. Our previous work shows the inhibition effects of spherical HA nanoparticles on U2-OS cell line [28,29], which makes it possible to use HA nanoparticles to fill the bone defects after tumor removal surgery. Due to the possible toxicity of the fine HA particles, cytotoxicity evaluation of the synthesized particles is essential.

In the present work, L929 cell line was chosen for the *in vitro* test. L929 cells were cultured for 1 and 10 days with 62.5, 125, 250, and 500 μg/mL commercial or nano HA particle and counted. The cells cultured without HA particles were treated as control group. The inhibition test results show (Figure 4) that both commercial and nano HA of different concentration have some inhibition effects on L929 cells at different time intervals. After 1 day (Figure 4(a)) in culture medium, the inhibition rate of both commercial HA and nano HA on L929 cells increases with an increasing concentration; there is no significant difference between them until the concentration reaches 500 μg/L, at which the commercial HA shows a greater inhibition effect on L929 cells than nano HA. After 10 days (see Figure 4(b)), except the suspension of 62.5 μg/mL, a less inhibition rate of nano HA than commercial HA was revealed at different concentrations. In addition, both particles showed a decreasing trend in inhibition rate with a longer time. These results demonstrate that nano HA is less toxic than the commercial HA and that the inhibition rate decreases with an increasing time.

Effects of Nanocrystalline Hydroxyapatite Particles on U2-OS Cell Proliferation

Figure 5 shows the measured inhibition rate for U2-OS bone osteosarcoma cell proliferation resulting from the presence of nanocrystalline HA particles in the culture medium. The inhibition rate depends on the time and on the concentration of the HA particles in the culture medium. At lower particle concentrations (31.25 and 62.5 μg/mL), the inhibition factor increases up to day 2 but then decreases by day 3, whereas for the higher particle concentrations, it increases continuously. The data indicate that there might be some threshold HA concentration below which inhibition cannot be sustained. At any time, the inhibition factor increases with increasing concentration

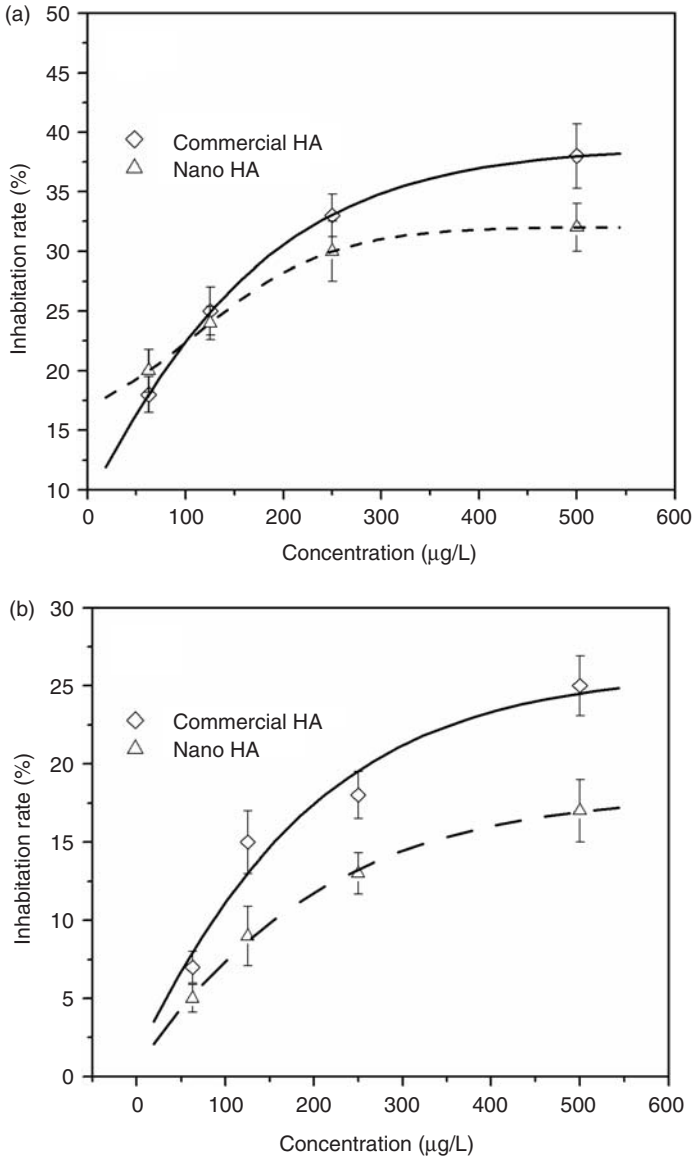

Figure 4. Growth inhibition effects of commercial and nano HA on L929 cell line at different time: (a) 1 day; and (b) 10 days.

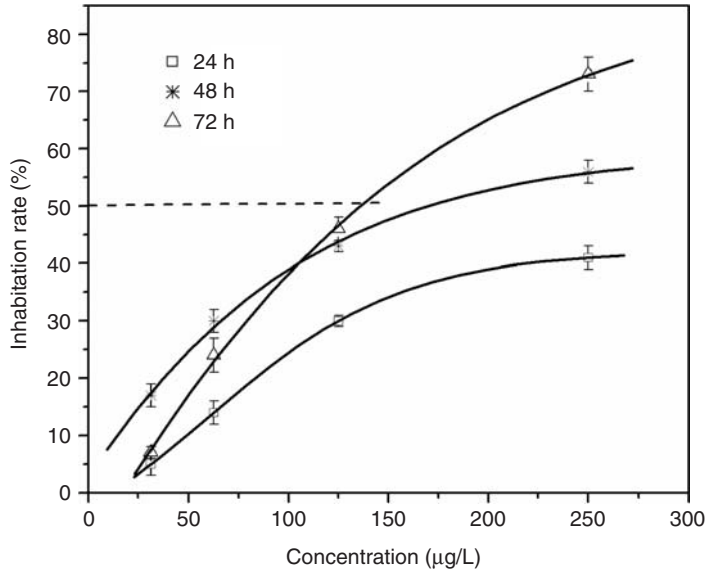

Figure 5. Growth inhibition effect of nano HA on U2-OS cancer cells.

of nanocrystalline HA in the culture medium and the IC50 of the particles was determined to be 50.8 μg/mL at 72 h.

TEM revealed that for the control group, the U2-OS cells had large, uniform nuclei, with uniform membranes (Figure 6(a)). In the trial group, cell shrinkage and nucleus condensation occurred, along with the presence of bubbles in the cytoplasm, indicating necrosis of the U2-OS cells (Figure 6(b)). Also the tache noirs, characteristics of necrotic area, were observed in the trial group.

Because of their fine particle size (20–40 nm) and high surface area (75 m^2/g), spherical nano-sized particles interact easily with malignant tumor cells. Nano-sized materials have been reported to enter tumors and distribute in several cytoplasmic organelles, including mitochondria, lysosome and dictyosome, but not enter nucleus [39]. Experiments have shown that nano-sized HA inhibited the proliferation of liver and paunch [8,9]. However, the effect of nano-sized HA particles on the metabolism of bone tumor cells has received little attention.

The results of the present work indicated that nanocrystalline HA particles in the culture medium inhibited the proliferation of U2-OS cells, and that cell shrinkage and cell wall desquamation occurred. Furthermore, the U2-OS cell morphology such as cell shrinkage, nucleus condensation, tache noirs and membrane rupture are indications of

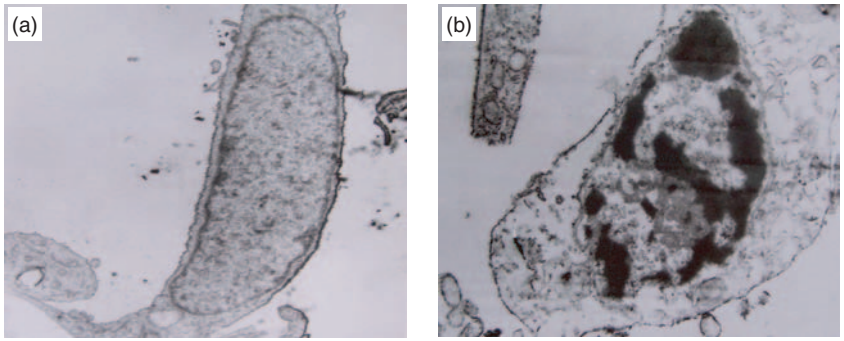

Figure 6. TEM of U2-OS bone osteosarcoma cells cultured for 3 days in (a) pure culture medium, and (b) culture medium containing 250 μg/mL nanocrystalline HA particles (×11,000).

cell necrosis. Therefore, it is highly likely that the inhibiting effect of nanocrystalline HA particles on U2-OS cell proliferation is caused by triggering cell necrosis.

Since calmodulin (CaM) at the surfaces of cancer cells is reported to be several times higher than the value at normal cells surfaces [40], the proliferation of cancer cells tend to be affected by the calcium ion concentration in the surrounding medium [41,42]. It is likely that calcium ions released from the spherical nanocrystalline HA leads to greater absorption of calcium ion into the cancer cells, leading to a lower cell growth rate. Because of the fine size of the spherical nanocrystalline HA particles used in the present work (20–40 nm), the particles have high solubility, high surface reactivity, high specific surface energy, and high capacity for ion exchange reaction. These characteristics promote reaction of the HA particles with the cancer cell surfaces, and enhance the potential for the particles to enter the cancer cells, leading to significant reduction in the proliferation of the U2-OS cancer cells.

CONCLUSION

L929 and U2-OS cell lines were used for *in vitro* measurement of the cell responses of a synthesized spherical HA nanoparticles (20–40 nm in diameter and 75 m^2/g in specific surface area). The synthesized nanoparticle shows a less or at least equal inhibition rate on L929 cell line and decreasing with increasing contact time, which demonstrates a less toxicity of synthesized HA than the commercial available HA. On the other hand, the inhibition rate of spherical HA nanoparticles on

U2-OS cell lines increases with increasing concentration and time and the IC50 of the particle was determined to be 50.8 μg/mL at 72 h.

ACKNOWLEDGMENTS

The authors would like to thank the Chinese Natural Science Foundation (NSF grant number 50272041) and the Nanotechnology Special Foundation of the Shanghai Science and Technology Committee (grant number 0144NM064) for financial support.

REFERENCES

1. Hench, L.L. (1991). Bioceramics: From Concept to Clinic, *J. Am. Ceram. Soc*., **74**(7): 1487–1510.
2. Wehanced, T.J., Ergun, C., Doremus, R.H., Siegel, R.W. and Bizios, R. (2000). Enhanced Functions of Osteoblasts on Nanophase Ceramics, *Biomaterials*, **21**(17): 1803–1810.
3. Suchanek, W. and Yoshimura, M. (1998). Processing and Properties of Hydroxyapatite-based Biomaterials for Use as Hard Tissue Replacement implants, *J. Mater. Res*., **13**(1): 84–117.
4. Hench, L.L. (1998). Bioceramics, *J. Am. Ceram. Soc*., **81**(7): 1705–1728.
5. Garvey, B.T. and Bizios, R. (1994). A Method for Transmission Electron Microscopy Investigation of the Osteoblast/Hydroxyapatite Interface, *J. Appl. Biomater*., **5**(1): 39–45.
6. Akao, M., Sakatsume, M., Aoki, H., Takagi, T. and Sasaki, T.S. (1993). In Vitro Mineralization in Bovine Tooth Germ Cell Cultured with Sintered Hydroxyapatite, *J. Mater. Sci. Mater. Med*., **4**(6): 569–574.
7. Puleo, D.A., Holleran, L.A., Doremus, R.H. and Bizios, R. (1991). Osteoblast Responses to Orthopedic Implant Materials In Vitro, *J. Biomed. Mater. Res*., **25**(6): 711–723.
8. Basle, M.F., Rebel, A., Grizon, F., Daculsi, G., Passuti, N. and Filman, R. (1993). Cellular Response to Calcium Phosphate Ceramics Implanted in Rabbit Bone, *J. Mater. Sci. Mater. Med*., **4**(3): 273–280.
9. Geesink, R.G.T., Groot, K.D.E. and Klein, C.P.A.T. (1988). Bonding of Bone to Apatite-Coated Implants, *J. Bone Joint Surg*., **70-B**(1): 17–22.
10. Jansen, J.A., Vander Waerden, J.P.C.M. and Wolke, J.G.C. (1993). A Histological Evaluation of the Effect of Hydroxyapatite Coating on Interfacial Response, *J. Mater. Sci. Mater. Med*., **4**(5): 466–470.
11. Klein, C.P.A.T., Patka, P., Wolke, J.G.C., de Blieck-Hogervorst, J.M.A. and de Groot, K. (1994). Long-term *In Vivo* Study of Plasma-Sprayed Coatings in Titanium Alloys of Tetracalcium Phosphate, Hydroxyapatite and A-Tricalcium Phosphate, *Biomaterials*, **15**(2): 146–150.
12. Wilke, A., Orth, J., Kraft, M. and Griss, P. (1993). Bone Ingrowth Behavior of Hydroxyapatite-Coated, Polyethylene-Intruded and Uncoated, Sandblasted Pure Titanium Implants in an Infected

Implantation Site: An experimental study in miniature pigs, *J. Mater. Sci. Mater. Med*., **4**(3): 260–265.

13. Oh, S.H., Finones, R.R., Daraio, C., Chen, L.H. and Jin, S.H. (2005). Growth of Nano-scale Hydroxyapatite Using Chemically Treated Titanium Oxide Nanotubes, *Biomaterials*, **26**(24): 4938–4943.
14. Ben-Nissan, B., Milev, A. and Vago, R. (2004). Morphology of Sol-gel Derived Nano-coated Coralline Hydroxyapatite, *Biomaterials*, **25**(20): 4971–4975.
15. Murugan, R. and Ramakrishna, S. (2004). Bioresorbable Composite Bone Paste Using Polysaccharide Based Nano Hydroxyapatite, *Biomaterials*, **25**(17): 3829–3835.
16. Cao, L.Y., Zhang, C.B. and Huang, J.F. (2005). Synthesis of Hydroxyapatite Nanoparticles in Ultrasonic Precipitation, *Ceram. Inter*., **31**(8): 1041–1044.
17. Tadic, D., Peter, F. and Epple, M. (2002). Continuous Synthesis of Amorphous Carbonated Apatites, *Biomaterials*, **23**(12): 2553–2559.
18. Philips, M.J., Darr, J.A., Luklinska, Z.B. and Rehman, I. (2003). Synthesis and Characterization of Nano-biomaterials with Potential Osteological Applications, *J. Mater. Sci. Mater. Med*., **14**(10): 875–882.
19. Evans, E.J. (1991). Toxicity of Hydroxyapatite in vitro: The Effect of Particle Size, *Biomaterials*, **12**(6): 574–576.
20. Sun, J.S., Tsuang, Y.H., Chang, W.H.S., Li, J., Liu, H.C. and Lin, F.H. (1997). Effect of Hydroxyapatite Particle Size on Myoblasts and Fibroblasts, *Biomaterials*, **18**(9): 683–690.
21. Ninomiya, J.T., Struve, J.A., Stelloh, C.T., Toth, J.M. and Crosby, K.E. (2001). Effects of Hydroxyapatite Particulate Debris on the Production of Cytokines and Proteases in Human Fibroblasts, *J. Orthop. Res*., **19**(4): 621–628.
22. Laquerriere, P., Grandjean-Laquerriere, A., Guenounou, M., Laurent-Maquin, D., Frayssinet, P. and Nardin, M. (2003). Correlation between Sintering Temperature of Hydroxyapatite Particles and the Production of Inflammatory Cytokines by Human Monocytes, *Colloid. Surf, B*, **30**(3): 207–213.
23. Laquerriere, P., Grandjean-Laquerriere, A., Jallot, E., Balossier, G., Frayssinet, P. and Guenounou, M. (2003). Importance of Hydroxyapatite Particles Characteristics on Cytokines Production by Human Monocytes *in vitro*, *Biomaterials*, **24**(16): 2739–2749.
24. Huang, J., Best, S.M., Bonfield, W., Brooks, R.A., Rushton, N., Jayasinghe, S.N. and Edirisinghe, M.J. (2004). *In vitro* Assessment of the Biological Response to Nano-sized Hydroxyapatite, *J. Mater. Sci. Mater. Med*., **15**(4): 441–445.
25. Grandjean-Laquerriere, A., Laquerriere, P., Laurent-Maqui, D., Guenounou, M. and Philips, T.M. (2004). The Effect of the Physical Characteristics of Hydroxyapatite Particles on Human Monocytes IL-18 Production *in vitro*, *Biomaterials*, **25**(28): 5921–5927.
26. Li, S.P. (1996). *Bioceramics*. Vol. 9, p. 225. Elsevier Science Inc., New York.
27. Liu, Z., Tang, S. and Ai, Z. (2003). Effects of Hydroxyapatite Nanoparticles on Proliferation and Apoptosis of Human Hepatoma BEL-7402 Cells, *World J. Gastroenterol*, **9**(9): 1968–1971.

28. Fu, Q., Zhou, N., Huang, W.H., Wang, D.P., Zhang, L.Y. and Li, H.F. (2004). Preparation and Characterization of a Novel Bioactive Bone Cement: Glass Based Nanoscale Hydroxyapatite Bone Cement, *J. Mater. Sci. Mater. Med*., **15**(12): 1333–1338.
29. Fu, Q., Zhou, N., Huang, W.H., Wang, D.P., Zhang, L.Y. and Li, H.F. (2005). Effects of Nano HAP on Biological and Structural Properties of Glass Bone Cement, *J. Biomed. Mater. Res*. *A*, **74A**(2): 156–163.
30. Mosmann, T. (1983). Rapid Colorimetric Assay for Cellular Growth and Survival: Application to Proliferation and Cytotoxicity Assays, *J. Immunol. Meth*., **65**(1–2): 55–63.
31. Heo, D.S., Park, J.G., Hata, K., Day, R., Herberman, R.B. and Whiteside, T.L. (1990). Evaluation of Tetrazolium-based Semiautomatic Colorimetric Assay for Measurement of Human Antitumor Cytotoxicity, *Cancer Res*., **50**(12): 3681–3690.
32. Kim, C.Y., Clark, A.E. and Hench, L.L. (1989). Early Stages of Calcium-phosphate Layer Formation in Bioglasses, *J. Non-Cryst. Solids*., **113**(2–3): 195–202.
33. Filho, O.P., LaTorre, G.P. and Hench, L.L. (1996). Effect of Crystallization on Apatite-layer Formation of Bioactive Glass 45S5, *J. Biomed. Mater. Res*., **30**(4): 509–514.
34. Posner, A.S., Blumenthal, N.C. and Betts, F. (1984). *Phosphate Minerals*., p. 330. Springer-Verlag, Berlin.
35. LeGeros, R.Z. and LeGeros, J.P. (1984). *Phosphate Minerals*, p. 352. Springer-Verlag, Berlin.
36. Huang, W., Day, D.E., Kittiratanapiboon, K. and Rahaman, M.N. (2006). Kinetics and Mechanisms of the Conversion of Silicate (45S5), borate, and Borosilicate Glasses to Hydroxyapatite in Dilute Phosphate Solutions, *J. Mater. Sci. Mate. Med*., **17**(7): 583–596.
37. Guthrie Jr., G.D. (1997). Mineral Properties and Their Contributions to Particle Toxicity, *Environ. Health Perspect*, **105**(S5): 1003–1011.
38. Blake, T., Castranova, V., Schwegler-Berry, D., Baron, P., Deye, G.J., Li, C. and Jones, W. (1998). Effect of Fiber Length on Glass Microfiber Cytotoxicity, *J. Toxicol. Environ. Health*, **54**(4): 243–259.
39. Savic, R., Luo, L.B., Eisenberg, A. and Maysinger, D. (2003). Micellar Nanocontainers Distribute to Defined Cytoplasmic Organelles, *Science*, **300**(5619): 615–618.
40. Wei, J.W., Morris, H.P. and Hickie, R.A. (1982). Positive Correlation Between Calmodulin Content and Hepatoma Growth Rates, *Cancer Res*., **42**(7): 2571–2574.
41. Schuller, H.M., Correa, E., Orloff, M. and Reznik, G.K. (1990). Successful Chemotherapy of Experimental Neuroendocrine Lung Tumors in Hamsters with an Antagonist of Calcium/calmodulin, *Cancer Res*., **50**(5): 1645–1649.
42. Strobl, J.S. and Peterson, V.A. (1992). Tamoxifen-resistant Human Breast Cancer Cell Growth: Inhibition by Thioridazine, Pimozide and the Calmodulin Antagonist, W-13, *J. Pharmacol. Exp. Ther*., **263**(1): 186–193.